

# Petrology, Geochemistry and Geochronology of Gabbros from the Zhongcang Ophiolitic Mélange, Central Tibet: Implications for an Intra-Oceanic Subduction Zone within the Neo-Tethys Ocean

Mengjing Xu, Cai Li\*, Wei Xu, Chaoming Xie, Peiyuan Hu, Ming Wang

College of Earth Science, Jilin University, Changchun 130061, China

**ABSTRACT:** In order to investigate the evolution of Shiquanhe-Yongzhu-Jiali ophiolitic mélange belt, the gabbros from new discovered Zhongcang ophiolitic mélange are studied through petrology, whole-rock geochemistry, zircon U-Pb dating and Lu-Hf isotope. The gabbros investigated in this paper contain cumulate gabbro and gabbro dike, and they have undergone greenschist-amphibolite facies metamorphism. The chondrite normalized rare earth element (REE) patterns of most of these rocks show flat types with slightly light REE (LREE) depletion and the N-MORB normalized incompatible elements diagrams indicate depletion in high field strength elements (HFSE) (Nb, Ta) and enrichment in large ion lithophile elements (LILE). These gabbros have island arc and mid-ocean ridge basalt affinities, suggesting that they were originated in an oceanic back arc basin. Whole rock geochemistry and high positive  $\varepsilon_{\text{Nd}}(t)$  values show that these gabbros were derived from ~30% partial melting of a spinel lherzolite mantle, which was enriched by interaction with slab-derived fluids and melts from sediment. U-Pb analyses of zircons from cumulate gabbro yield a weighted mean age of  $114.3 \pm 1.4$  Ma. Based on our data and previous studies, we propose that an intra-oceanic subduction system and back arc basin operated in the Neo-Tethys Ocean of central Tibet during Middle Jurassic and Early Cretaceous, resembling modern active intra-oceanic subduction systems in the western Pacific.

**KEY WORDS:** Tibet, Zhongcang ophiolitic mélange, gabbro, Shiquanhe-Yongzhu-Jiali ophiolitic mélange belt, geochemistry.

## 1 INTRODUCTION

Ophiolites are useful in reconstruction of the tectonic history of a region, as these units indicate the presence of sutures and the closure of ancient oceanic basins (Savov et al., 2001). Gabbros are an integral part of the crustal section in an ophiolitic suite, and they are created by the injection of basaltic melt from the underlying rising mantle (Kakar et al., 2013). The gabbros record the succession of magmatic events from deep to shallow crustal levels. Therefore, the study of gabbros is a key for evaluating the evolution of the oceanic lithosphere (Ray et al., 2011).

Shiquanhe-Yongzhu-Jiali ophiolitic mélange belt (SYJMB) lies in the central Tibet, and it extends from Shiquanhe in the west to Chayu in the east, for about least 1 000 km length (Fig. 1a) (Pan et al., 2012). The SYJMB is generally thought to be obduction southward production during closure of the Bangong-Nujiang Ocean (Zhang, 2007; Kapp et al., 2003;

Coward et al., 1988; Girardeau et al., 1985, 1984). However, other workers debated that the SYJMB represented a Late Jurassic to Early Cretaceous back-arc basin of the Bangong-Nujiang suture zone (BNZS) (e.g., Geng et al., 2011; Zhu et al., 2011; Pan et al., 2006; Hu, 1990). This controversy is a result of the absent of systematic and detailed studies of the ophiolitic mélanges in SYJMB, although the tectonic environment and geodynamic significance of the Lagkorco ophiolitic mélange in the western portion of the SYJMB is relatively well known.

Previous studies of the SYJMB ophiolitic mélanges have focused mostly on the field characteristics (e.g., Zheng et al., 2004; Kapp et al., 2003), radiometric ages (e.g., Zeng et al., 2006; Wang et al., 2003), isotope dating and the geochemistry of the volcanic rocks (e.g., Zhang, 2007; Ye et al., 2005; Yang et al., 2003). In this study, we focus on gabbros from the newly discovered Zhongcang ophiolitic mélange in the western part of SYJMB. We performed detailed petrological, whole rock geochemical investigations, as well as zircon U-Pb dating and Lu-Hf isotope analysis. The results are used to: (1) elucidate the origin of these gabbros and the nature of the petrological processes; (2) determine the tectonic setting of the Zhongcang ophiolitic mélange; and (3) compare its tectonic setting with those of other ophiolitic mélange massifs along the whole SYJMB.

\*Corresponding author: licai010@126.com

© China University of Geosciences and Springer-Verlag Berlin Heidelberg 2014

Manuscript received September 25, 2013.

Manuscript accepted January 20, 2014.

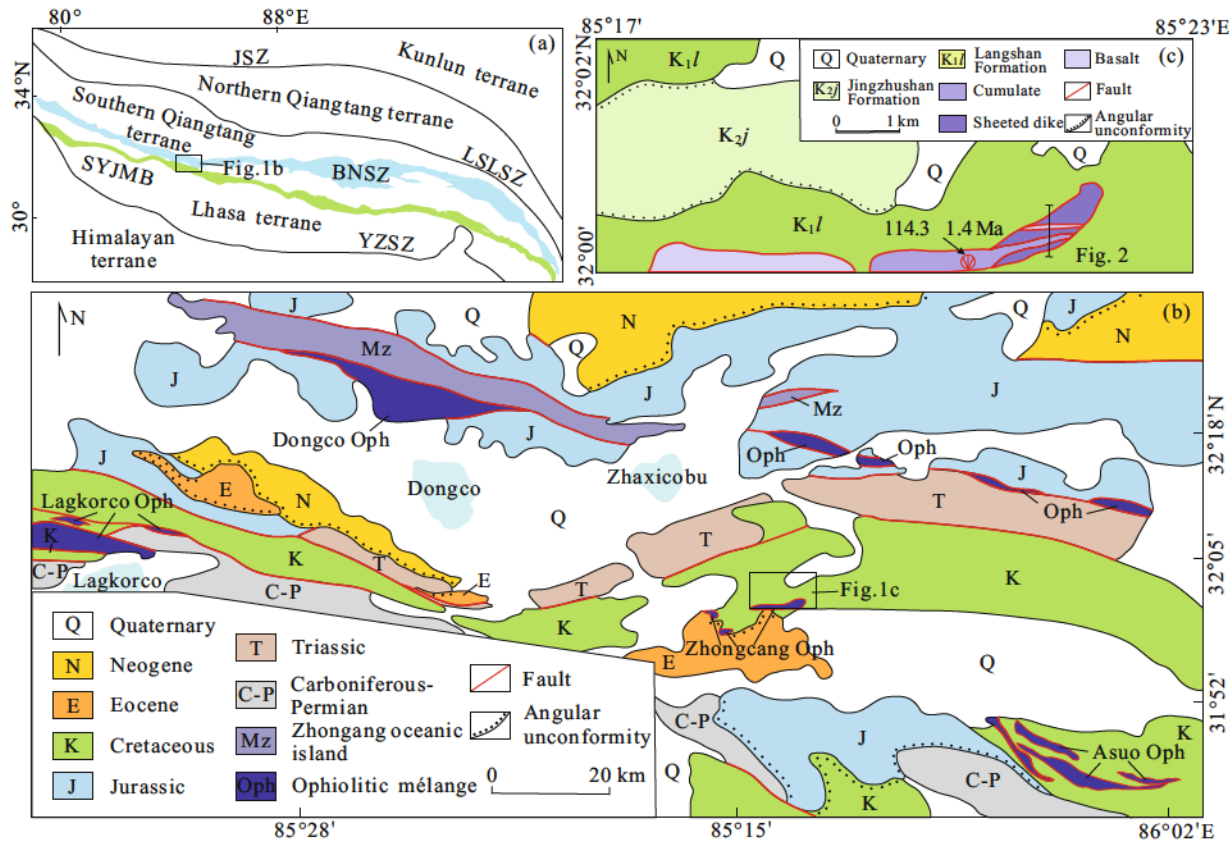


**Figure 1.** (a) Simplified tectonic map of the Tibetan Plateau showing major sutures (modified from Li et al., 2009; Pan et al., 2004; Yin and Harrison, 2000). The major sutures are: JSZ. Jinshajiang suture zone; BNSZ. Bangong-Nujiang suture zone; SYJMB. Shiquanhe-Yongzhu-Jiali ophiolitic mélange belt; YZSZ. Yarlung-Zangbo suture zone; LSLSZ. Longmuo-Shuanghu-Lancang suture zone; (b) Schematic geological map of the Zhongcang area showing the ophiolitic massifs within the BNSZ and SYJMB based on Zeng et al. (2011, 2006), Liu et al. (2003), and Xie et al. (2002). Oph. Ophiolite; (c) simplified geological map showing the gabbros of Zhongcang ophiolitic mélange discussed in this study.

## 2 GEOLOGICAL SETTING

The Tibetan Plateau is an amalgamation of terranes that were accreted in a southward younging fashion (e.g., Mattern and Schneider 2000; Dewey et al., 1988). From north to south, they are the Qiadam, Bayankala-Ganzi, northern Qiangtang, southern Qiangtang, Lhasa and Himalayan terranes (Fig. 1a). These terranes are separated by a series of suture zones, i.e., the Kunlun, Jinsha, Longmuo-Shuanghu-Lancang, Bangong-Nujiang and Yarlung-Zangbo suture zones (Fig. 1a) (e.g., Yin and Harrison, 2000; Li, 1987). The Shiquanhe-Yongzhu-Jiali ophiolitic mélange belt separates northern Lhasa subterrane to the north from central Lhasa subterrane to the south (Zhu et al., 2011).

The SYJMB is mainly composed of ophiolitic fragments and mélanges, which include pre-Ordovician metamorphic rocks, Permian limestone, Jurassic to Early Cretaceous limestones and so on (e.g., Pan et al., 2006; Zheng et al., 2004; Wang et al., 2003). No associated flysch sediment has been discovered (Pan et al., 2006), and the ophiolitic mélanges tectonically rest on strata of different times (e.g., He et al., 2006; Ye et al., 2004).

Zhongcang ophiolitic mélange located in about 500 m south of Zhongcang Country, Nima Town is oriented in an E-W direction. It is about 8 km long and has a maximum width of

about 1.5 km (Fig. 1b). The ophiolitic sequence mainly consists of metamorphic peridotite, cumulate gabbro and gabbro dike, and occurs as sheets within Early Cretaceous Langshan Formation. The Langshan Formation is mainly composed of limestone with orbitolina fossils, and unconformably overlain by Late Cretaceous Jingzhushan Formation in the north and Eocene in the south (Fig. 1b). Metamorphic peridotites are exposed chiefly in the western part of Zhongcang ophiolitic mélange. They are associated with red chert, brecciated peridotite, gabbro and diabase (Liu et al., 2003). The eastern part of Zhongcang ophiolitic sequence has well developed cumulate gabbros and gabbro dikes with minor basalts, and they are in fault contact (Figs. 1c and 2). The gabbro dikes are generally 10–100 cm widths. The cumulate gabbros and gabbro dikes investigated in this paper are collected from the eastern part of Zhongcang ophiolitic mélange.

## 3 PETROLOGY

Zhongcang ophiolitic rocks have been variably altered. The mantle peridotites exhibit strong foliations and are extensively serpentinized with pyroxene replaced by bastite and olivine by serpentine and secondary magnetite (Liu et al., 2003). Spinel grains are the least altered, whereas many grains are partly to completely replaced by magnetite (Liu et al., 2003). The

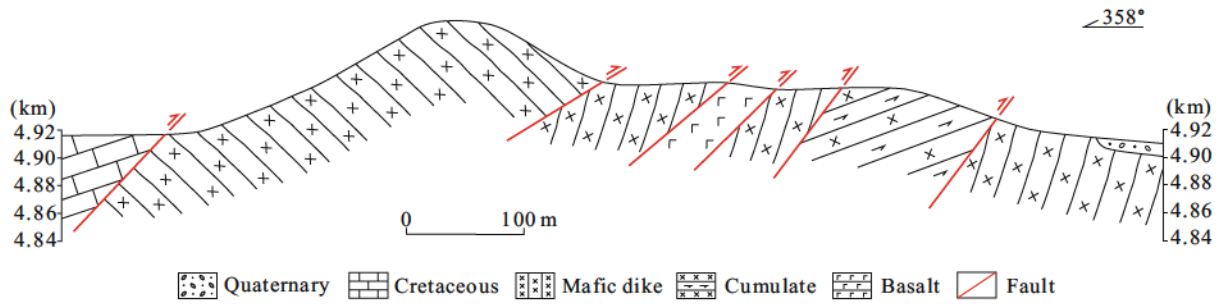


**Figure 2.** Detailed geological cross-section of Zhongcang ophiolitic mélange. The location of profile is shown in Fig. 1c.

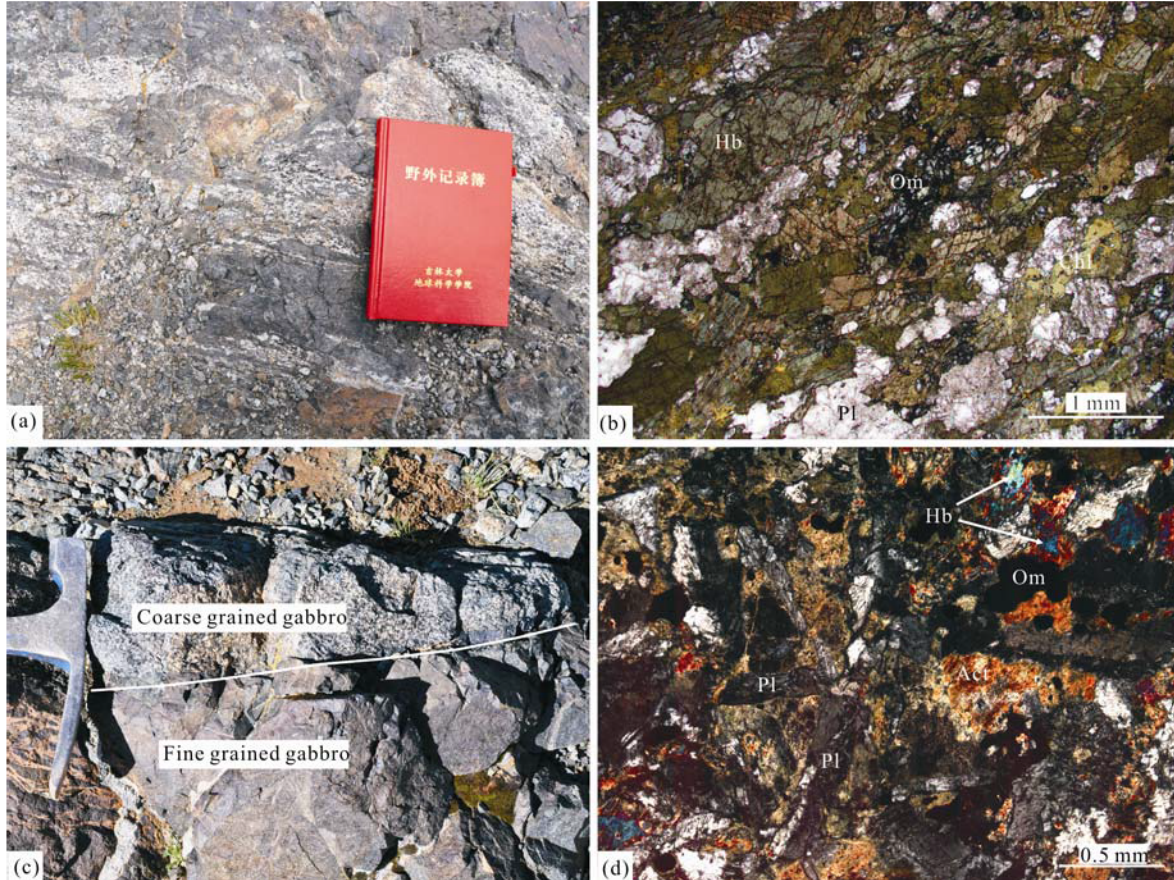


**Figure 3.** Petrologic characteristics of gabbros of Zhongcang ophiolitic mélange. (a) Meta-cumulate gabbro; (b) amphibolite and chlorite replacing pyroxene; (c) gabbro dikes including coarse grained and fine grained gabbros; (d) gabbroic texture of gabbro with amphibolite and actinolite replacing pyroxene. Hb. amphibolite; Pl. plagioclase; Chl. chlorite; Act. actinolite; Om. opaque mineral.

cumulate gabbros have undergone greenschist-amphibolite facies metamorphism, but cumulate structure can be found in some place (Fig. 3a). The mineral assemblages of the cumulate gabbros are mainly amphibolite, plagioclase, chlorite and opaque mineral (Fig. 3b). However, minor remnant pyroxene can be observed. The dikes show variable mineral grain sizes and fined-grained gabbros are interbedded with coarse grained gabbros (Fig. 3c). The gabbro dike typically shows a gabbroic texture with platy labradoritic plagioclase and prismatic amphibolite and actinolite crystals replacing the pyroxene (Fig. 3d). Opaque minerals are present in minor to accessory amounts.

#### 4 ANALYTICAL TECHNIQUES

Whole rock elements compositions of samples were analyzed at ICP-OES and LA-ICP-MS laboratories, China University of Geoscience (Beijing). Major element abundances were determined using PS-950 X-ray fluorescence spectrometry (XRF). The agatecrushed sample was dried first at 106 °C for 2–4 h. After it, 25 g of the annealed sample was mixed with 5 g of sodium tetraborate in platinum crucible. This mixture was melted in high frequency furnace. After cooling, the melt was diluted to 100 mL by adding water. The analytical precision (relative standard deviation) is usually 1% for SiO<sub>2</sub>, 4%–10% for other oxides (Yu, 2011). Whole rock trace element compositions were analyzed by Agilent 7 500 a inductively coupled

plasma emission mass spectrometry (ICP-MS). About 50 mg samples were dissolved in a mixture of HF and HNO<sub>3</sub> in bombs at 195 °C for 48 h. This procedure was repeated using larger amounts of acids at 165 °C for 24 h. After digestion, the sample was diluted with Milli-Q water to a final dilution factor of 2000. The AGV-2 (US Geological Survey) and GSR-3 (National Geological Standard Reference Materials of China) standards were used to monitor the analytical accuracy. These results indicate that the accuracy is better than 5% for trace elements. Analytical details and analysis of reference materials are reported in Yu (2011).

High spatial resolution U-Th-Pb elements and isotopic ratios of zircon were generated using a laser-ablation inductively coupled plasma mass spectrometer (LA-ICP-MS) at the LA-ICP-MS Laboratory, China University of Geoscience (Beijing). The zircons were collected in Geological Survey of Hebei Province. The best quality zircon grains, characterized by homogeneity, transparency, homogeneous color, fluorescence and absence of inclusions were picked for dating. Zircon grains were mounted together with epoxy on a disk, and polished to obtain an even surface. The internal texture of zircons was observed using cathodoluminescence (CL) images carrying out in Physics College, Peking University. Zircons were dated in-situ on the LA-ICP-MS. The laser-ablation system is an UP 193SS equipped with a 193 nm ArF-excimer laser, and a homogenizing and imaging optical system. Zircon U-Th-Pb elements and isotopic ratios were analyzed on the Agilent 7500a ICP-MS, and a 30 μm diameter spot for the laser ablation of a single grain. <sup>207</sup>Pb/<sup>206</sup>Pb, <sup>206</sup>Pb/<sup>238</sup>U, <sup>237</sup>Pb/<sup>235</sup>U and <sup>208</sup>Pb/<sup>232</sup>Th ratios were calculated using GLITTER 4.4 (Macquarie University), and were corrected for both instrumental mass bias and depth-dependent elemental and isotopic fractionation using Harvard zircon 91500 as an external standard. The ages were calculated using ISOPLOT (Ludwig, 2000). Compositions of the common Pb component were corrected following the method of Andersen (2002). Age uncertainties were quoted at the 95% confidence level.

A total of 17 dated zircon grains were selected for Lu and Hf isotopic analyses using LA-MC-ICP-MS at the State Key

Laboratory of Geological Processes and Mineral Resources, China University of Geosciences (Wuhan). A Neptune Plus MC-ICP-MS instrument was used to acquire time resolved signals. The detailed instrumental parameters of the laser-ablation system (GeoLas 2005) and MC-ICP-MS are described by Liu et al. (2012) and Hu et al. (2012).

## 5 RESULTS

### 5.1 Geochemistry

Table 1 includes the results of major, trace and rare earth elements analyses of the gabbros from the Zhangcang ophiolitic mélange. All samples have high (>6 wt.%) MgO and low (<54 wt.%) SiO<sub>2</sub> contents and are therefore fairly mafic in composition (Table 1). They range from basalts to andesites and belong to the subalkaline rock series based on the major oxide as well as resistant trace-element compositions (Fig. 4a). Figure 4b shows a SiO<sub>2</sub>-FeOT/MgO plot of the gabbros of the Zhongcang ophiolitic mélange. Most of the samples plot in the tholeiitic field, but few straddle the tholeiitic-calc-alkaline boundary. The cumulate gabbros and gabbro dikes display similar geochemical evolution as demonstrated by the Fig. 5. However, there are also notable differences. Cumulate gabbros have higher SiO<sub>2</sub> than gabbro dikes. In terms of trace elements, the cumulate gabbros have lower Cr and Ni absolute concentrations for given MgO values than gabbro dikes. These plots show a linear relationship with various degree of scatter (Fig. 5). These trends show that all the gabbros were probably formed from an identical parental magma. The crystallization of plagioclase alone can result in the depletion of SiO<sub>2</sub> and enrichment of MgO of residual magmas (Scoates, 2000). Therefore, it is probably caused by plagioclase cumulate during mafic magma evolution that the gabbro dikes have more mafic compositions than cumulate gabbros.

Most of the gabbros have flat REE patterns with slight depletion in the most incompatible LREE (normalized to chondrite), similar to normal MORB (Figs. 6a, 6b). Only one sample of cumulate gabbros has slightly LREE-enriched pattern (Fig. 6a). Some samples have REE content lower than that of N-MORB (Figs. 6a, 6b). The slightly positive Eu anomalies in

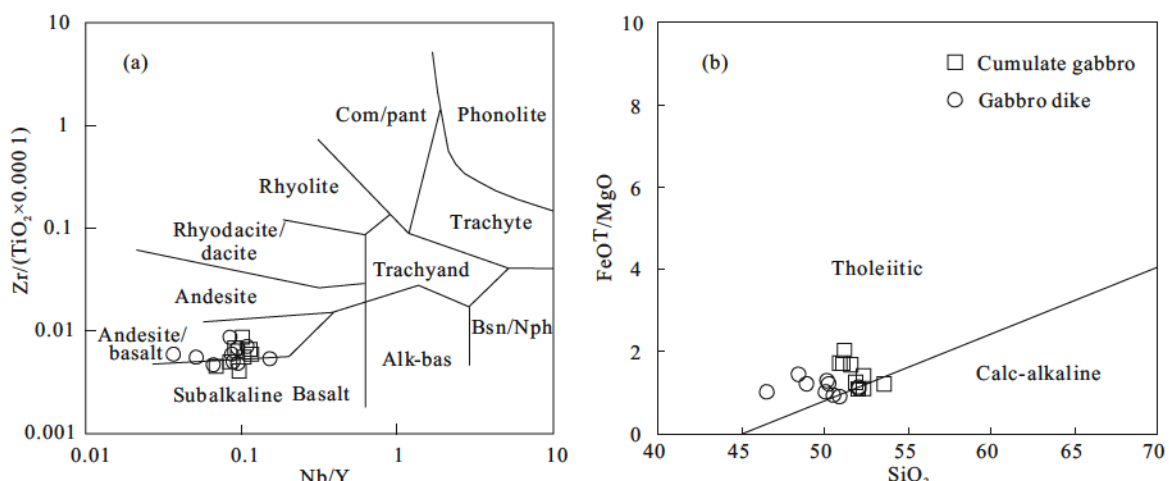


**Figure 4. Geochemical classification for the gabbros. (a)** Diagram of Zr/(TiO<sub>2</sub>×0.000 1) versus Nb/Y (after Winchester and Floyd, 1977); **(b)** plot of SiO<sub>2</sub> versus FeOT/MgO. The boundary line between tholeiitic and calc-alkaline rock types is from Miyashiro (1974).

**Table 1 The concentration of major (wt.%), trace elements (ppm) and their parameters for cumulate gabbros (dP1703) and gabbro dikes (DC12T21)**

Sample No.	dP1703H1	dP1703H4	dP1703H9	dP1703H2	dP1703H5	dP1703H8	dP1703H10	dP1703H3	dP1703H7
SiO <sub>2</sub>	52.08	53.64	52.42	51.65	51.17	51.00	52.36	51.87	51.26
TiO <sub>2</sub>	0.80	0.63	0.77	1.85	1.91	1.94	1.52	1.39	2.06
Al <sub>2</sub> O <sub>3</sub>	14.98	18.94	15.31	13.69	13.51	13.15	14.29	14.64	13.37
Fe <sub>2</sub> O <sub>3</sub> <sup>T</sup>	8.87	6.42	8.20	11.86	12.24	12.09	10.56	9.80	13.04
MnO	0.15	0.10	0.14	0.19	0.19	0.18	0.19	0.13	0.23
MgO	7.51	4.83	6.87	6.50	6.43	6.40	6.77	7.25	5.89
CaO	11.07	9.64	11.57	9.06	9.52	10.45	9.04	10.26	9.04
Na <sub>2</sub> O	2.74	3.90	2.83	3.21	2.65	2.44	3.03	2.80	3.08
K <sub>2</sub> O	0.15	0.17	0.16	0.10	0.11	0.09	0.15	0.18	0.10
P <sub>2</sub> O <sub>5</sub>	0.04	0.03	0.05	0.18	0.19	0.18	0.15	0.12	0.20
LOI	0.90	0.88	0.92	0.85	1.29	1.30	1.05	0.82	0.89
Total	99.27	99.19	99.23	99.16	99.20	99.22	99.11	99.26	99.15
Li	0.83	1.67	0.72	0.35	7.03	1.38	1.28	1.93	0.13
P	259	203	290	944	2 056	921	802	642	1 090
K	1 630	1 821	1 650	1 098	2 348	967	1 652	1 787	1 654
Sc	44.02	25.22	41.55	37.36	80.36	38.32	36.66	37.26	40.84
Ti	4 424	3 490	4 137	10 190	22 380	10 672	8 516	7 634	11 804
V	231	162	227	303	655	319	262	264	360
Cr	133	73.94	142	138	343	150	192	234	105
Mn	1 082	733	1 023	1 413	2 866	1 341	1 436	938	1 800
Co	35.62	25.50	31.65	35.86	77.60	36.22	39.54	36.46	41.08
Ni	62.62	47.82	53.89	56.46	129	59.30	69.26	83.82	48.88
Cu	24.68	46.80	12.07	37.12	81.58	58.72	223	4.34	155.10
Zn	58.78	39.70	41.99	48.74	93.74	54.74	76.34	45.28	194
Ga	14.32	15.72	13.75	15.69	30.68	15.12	15.30	14.76	17.98
Rb	2.73	3.36	2.84	1.33	3.68	1.11	3.23	1.94	2.43
Sr	172	245	174	174	324	109	178	169	179
Y	16.71	11.02	15.79	36.48	66.22	33.12	30.04	25.54	43.14
Zr	34.85	30.36	42.04	120	165	77.53	93.57	82.10	137
Nb	1.16	0.95	1.66	4.17	6.90	3.29	2.92	3.00	3.95
Cs	2.47	2.17	2.37	0.93	1.36	0.31	1.26	1.63	0.49
Ba	9.75	13.85	9.78	8.92	13.69	5.34	7.67	8.77	7.62
La	1.57	1.86	1.60	4.72	7.56	3.57	3.85	2.97	5.32
Ce	4.67	4.40	4.57	13.62	22.72	10.91	11.15	8.83	15.49
Pr	0.79	0.65	0.76	2.27	3.82	1.86	1.82	1.45	2.53
Nd	4.44	3.34	4.23	12.12	21.16	10.43	9.74	7.92	13.67
Sm	1.65	1.12	1.54	4.01	7.19	3.58	3.21	2.71	4.59
Eu	0.76	0.78	0.73	1.36	2.68	1.27	1.16	0.96	1.60
Gd	2.36	1.54	2.20	5.28	9.65	4.81	4.28	3.66	6.14
Tb	0.43	0.28	0.40	0.94	1.69	0.85	0.76	0.65	1.10
Dy	2.90	1.86	2.71	6.24	11.31	5.69	5.07	4.38	7.33
Ho	0.61	0.40	0.57	1.31	2.37	1.19	1.07	0.92	1.54
Er	1.77	1.15	1.66	3.85	6.87	3.49	3.12	2.73	4.54
Tm	0.25	0.17	0.24	0.55	0.96	0.49	0.45	0.39	0.65
Yb	1.63	1.09	1.51	3.57	6.21	3.16	2.87	2.53	4.26
Lu	0.24	0.16	0.22	0.52	0.90	0.47	0.43	0.37	0.62
Hf	0.87	0.78	1.09	2.91	4.09	2.02	2.28	2.02	3.37
Ta	0.07	0.07	0.19	0.26	0.42	0.20	0.18	0.20	0.25
Pb	0.09	0.66	0.47	0.24	0.67	0.67	0.36	0.23	0.86
Th	0.29	0.39	0.31	0.43	0.33	0.20	0.35	0.30	0.49
U	0.04	0.07	0.05	0.10	0.14	0.08	0.08	0.07	0.11
Mg <sup>#</sup>	66.36	63.66	66.15	56.08	55.05	55.22	59.91	63.29	51.28
Eu/Eu*	1.18	1.82	1.21	0.90	0.99	0.93	0.96	0.93	0.92
ΣREE	24.05	18.78	22.93	60.36	105.10	51.77	48.97	40.49	69.37
La/Yb	0.96	1.71	1.06	1.32	1.22	1.13	1.34	1.17	1.25
Dy/Yb	1.78	1.71	1.79	1.75	1.82	1.80	1.77	1.73	1.72

## Continued

Sample No.	dP1703H1	dP1703H4	dP1703H9	dP1703H2	dP1703H5	dP1703H8	dP1703H10	dP1703H3	dP1703H7
Sample No.	DC12T21 H1	DC12T21 H2	DC12T21 H3	DC12T21 H4	DC12T21 H5	DC12T21 H6	DC12T21 H7	DC12T21 H8	DC12T21 H9
La/Sm	0.95	1.66	1.04	1.18	1.05	1.00	1.20	1.09	1.16
Sm/Yb	1.01	1.03	1.02	1.12	1.16	1.13	1.12	1.07	1.08
Nb/Yb	0.71	0.87	1.10	1.17	1.11	1.04	1.02	1.18	0.93
Sr/Nd	38.73	73.31	41.06	14.36	15.30	10.45	18.25	21.28	13.08
Th/Yb	0.18	0.36	0.20	0.12	0.05	0.06	0.12	0.12	0.11
SiO <sub>2</sub>	50.13	52.11	46.58	50.20	49.00	48.46	51.00	52.07	50.61
TiO <sub>2</sub>	0.70	1.62	0.54	1.69	1.75	1.78	0.68	1.97	0.54
Al <sub>2</sub> O <sub>3</sub>	16.38	14.16	19.34	15.56	16.22	14.30	15.97	15.32	17.89
Fe <sub>2</sub> O <sub>3</sub> <sup>T</sup>	8.83	8.10	8.07	9.74	8.24	10.94	7.19	7.92	7.15
MnO	0.15	0.15	0.14	0.16	0.16	0.17	0.13	0.15	0.11
MgO	8.07	6.72	7.33	6.93	6.21	6.81	7.34	6.26	7.05
CaO	11.01	11.23	11.27	9.46	12.12	11.38	11.60	10.41	10.70
Na <sub>2</sub> O	3.20	3.79	3.40	4.28	3.50	3.28	3.50	4.16	3.55
K <sub>2</sub> O	0.07	0.17	0.15	0.19	0.13	0.12	0.19	0.12	0.18
P <sub>2</sub> O <sub>5</sub>	0.03	0.11	0.04	0.11	0.10	0.15	0.04	0.13	0.04
LOI	1.04	1.42	1.91	1.28	1.64	2.29	1.96	1.06	1.76
Total	99.62	99.58	98.77	99.60	99.07	99.68	99.60	99.56	99.57
Li	1.32	3.44	5.39	2.63	4.20	3.86	3.69	1.94	3.58
P	143	511	137	536	467	654	168	524	143
K	610	1 435	1 203	1 637	1 032	855	1 517	956	1 312
Sc	47.94	45.64	35.59	45.32	44.18	42.54	48.54	43.28	34.30
Ti	4 474	10 310	3 150	11 432	10 184	11 026	4 106	11 980	3 342
V	211	281	170	365	292	296	197	257	145
Cr	228	172	270	286	187	176	215	263	282
Mn	1 125	1 154	997	1 274	1 253	1 215	924	1 085	777
Co	37.58	27.22	38.31	37.02	29.28	37.96	29.44	25.64	30.84
Ni	77.26	58.76	86.50	86.60	68.50	72.58	64.06	69.90	94.86
Cu	15.47	10.49	129	7.64	3.61	51.26	23.50	3.09	17.78
Zn	41.86	37.90	42.12	41.22	35.58	37.60	37.70	24.36	33.76
Ga	17.12	16.72	17.05	20.32	18.93	17.97	14.54	17.11	15.42
Rb	1.39	5.57	4.95	5.33	3.66	2.73	6.68	3.75	5.94
Sr	184	232	201	250	237	203	232	251	209
Y	25.34	39.58	13.68	57.58	46.82	38.24	19.64	41.34	13.08
Zr	41.04	107	28.53	143	122	88.11	36.59	92.47	25.04
Nb	0.93	3.79	2.11	4.95	5.12	3.40	1.03	3.99	0.88
Cs	0.55	1.11	1.42	0.67	0.48	0.30	1.59	0.78	0.95
Ba	9.45	14.34	10.43	14.06	12.15	9.04	10.67	11.60	10.41
La	1.82	4.78	1.09	6.82	4.23	4.43	1.55	4.78	1.45
Ce	5.79	14.30	3.23	21.96	13.28	13.91	4.97	14.66	4.19
Pr	1.07	2.32	0.59	3.77	2.39	2.39	0.90	2.51	0.70
Nd	6.19	11.94	3.40	19.51	13.16	12.22	5.12	13.23	3.77
Sm	2.44	4.04	1.30	6.48	4.70	4.14	1.96	4.53	1.31
Eu	1.06	1.34	0.75	1.85	1.51	1.35	0.81	1.37	0.73
Gd	3.51	5.37	1.91	8.30	6.42	5.43	2.76	6.05	1.91
Tb	0.64	0.96	0.34	1.48	1.14	0.95	0.45	1.07	0.34
Dy	4.36	6.50	2.35	9.66	7.74	6.32	3.30	7.01	2.23
Ho	0.93	1.38	0.49	2.07	1.63	1.35	0.72	1.50	0.48
Er	2.70	4.10	1.44	6.12	4.89	3.98	2.03	4.38	1.40
Tm	0.38	0.59	0.20	0.89	0.69	0.56	0.29	0.62	0.19
Yb	2.42	3.92	1.32	5.59	4.57	3.63	1.82	3.96	1.25
Lu	0.36	0.59	0.19	0.83	0.66	0.55	0.27	0.59	0.19
Hf	1.21	2.73	0.70	3.72	2.87	2.32	1.00	2.59	0.70
Ta	0.05	0.24	0.17	0.30	0.53	0.21	0.07	0.23	0.07

Continued

Sample No.	DC12T21 H1	DC12T21 H2	DC12T21 H3	DC12T21 H4	DC12T21 H5	DC12T21 H6	DC12T21 H7	DC12T21 H8	DC12T21 H9
Pb	0.73	0.76	0.48	0.46	0.51	0.71	0.31	0.43	0.65
Th	0.05	0.33	0.07	0.44	0.23	0.26	0.04	0.30	0.06
U	0.02	0.10	0.05	0.10	0.06	0.06	0.04	0.07	0.04
Mg <sup>#</sup>	68.04	65.93	67.94	62.39	63.73	59.19	70.41	64.81	69.71
Eu/Eu*	1.11	0.88	1.45	0.77	0.84	0.87	1.06	0.80	1.42
ΣREE	33.66	62.12	18.61	95.33	67.01	61.21	26.96	66.26	20.15
La/Yb	0.75	1.22	0.83	1.22	0.93	1.22	0.85	1.21	1.16
Dy/Yb	1.80	1.66	1.78	1.73	1.69	1.74	1.81	1.77	1.78
La/Sm	0.74	1.18	0.84	1.05	0.90	1.07	0.79	1.05	1.11
Sm/Yb	1.01	1.03	0.98	1.16	1.03	1.14	1.08	1.14	1.05
Nb/Yb	0.39	0.97	1.60	0.88	1.12	0.94	0.56	1.01	0.70
Sr/Nd	29.68	19.45	58.97	12.80	17.99	16.58	45.43	18.99	55.33
Th/Yb	0.02	0.08	0.05	0.08	0.05	0.07	0.02	0.08	0.04

Note: Mg<sup>#</sup>=100×Mg<sup>2+</sup>/(Mg<sup>2+</sup>+Fe<sup>2+</sup>); Eu/Eu\*=Eu<sub>N</sub>/SQRT(Sm<sub>N</sub>×Gd<sub>N</sub>).

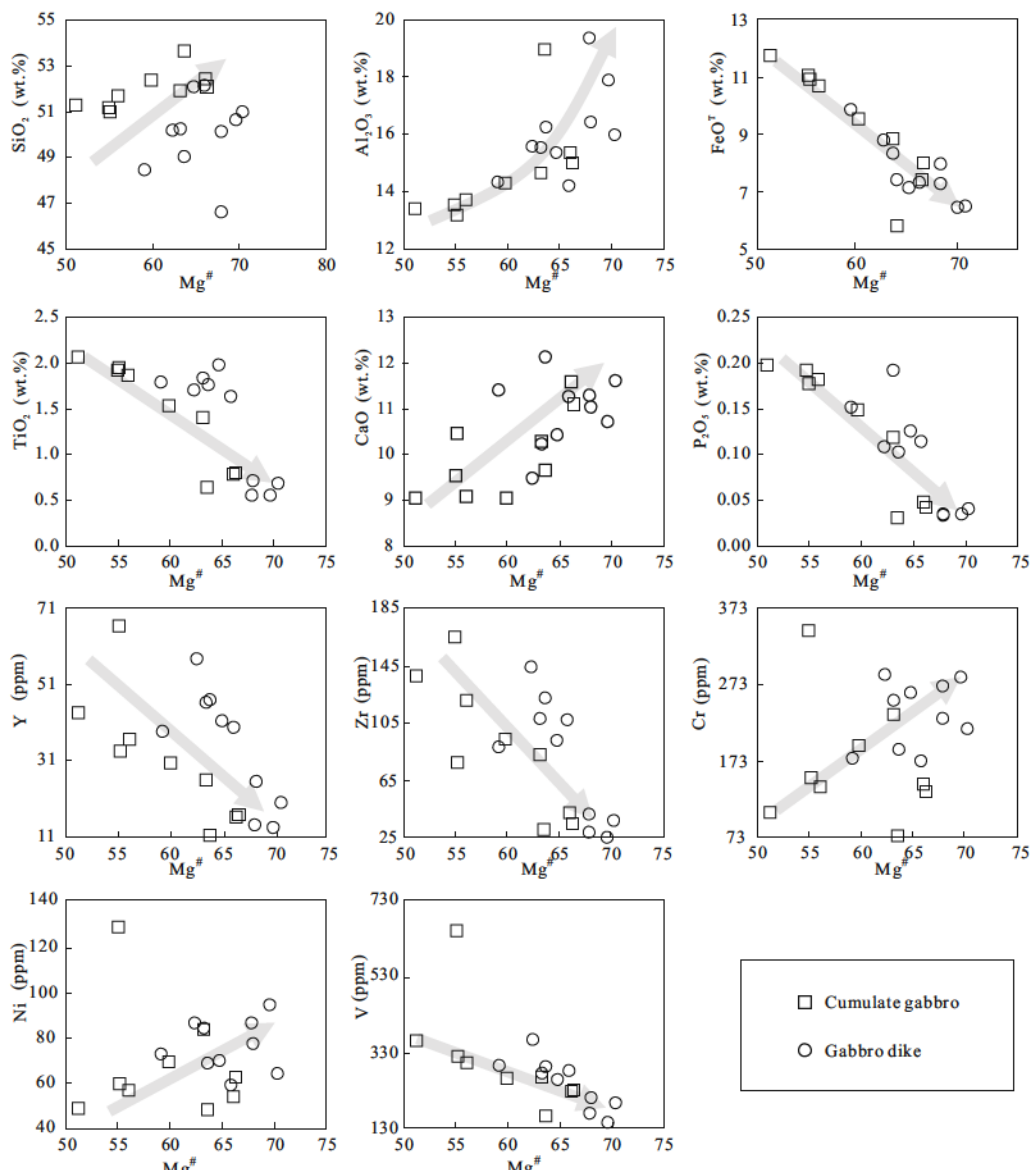


**Figure 5.** Representative major and trace elements plotted against Mg<sup>#</sup> showing the geochemical relationships between cumulate gabbro and gabbro dike. Values are in ppm for elements and in wt.% for oxides.

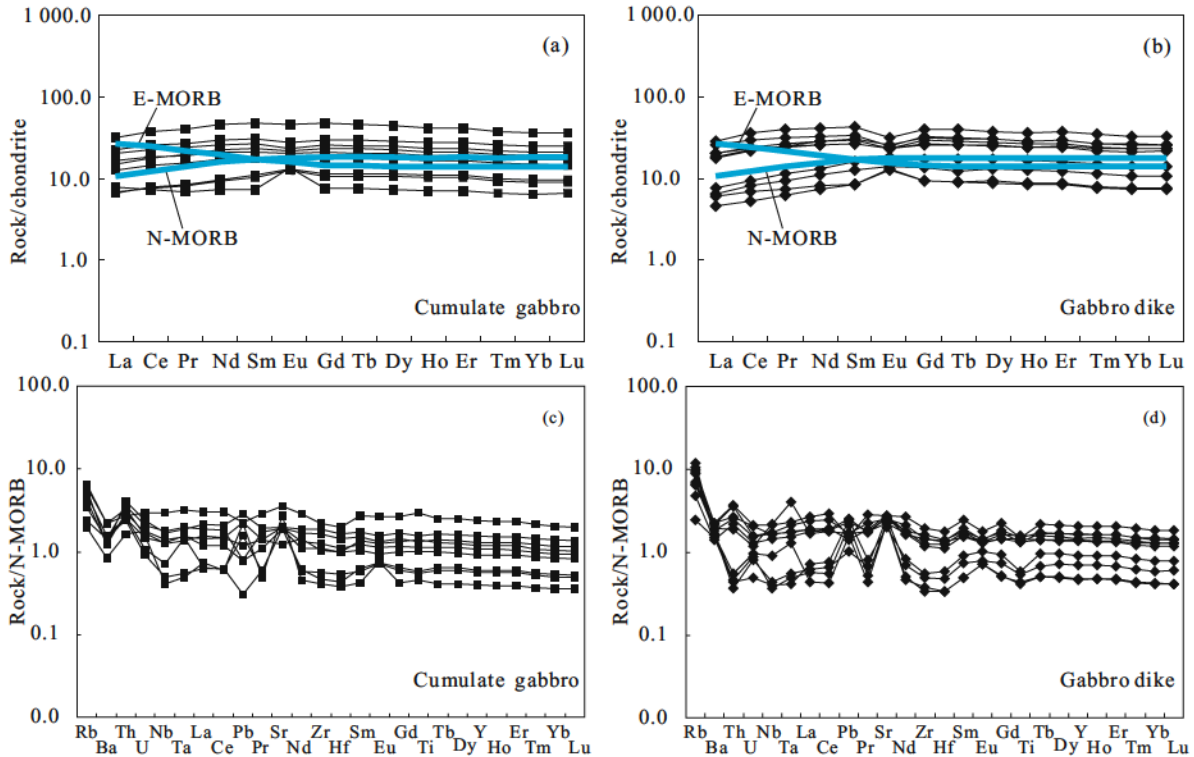


**Figure 6. Chondrite-normalized REE diagrams and N-MORB normalized spider diagrams for cumulate gabbros (a), (c) and gabbro dikes (b), (d) (normalizing values are from Sun and McDonough, 1989).**

some samples suggest plagioclase accumulation. The total range of REE concentrations of cumulate gabbros and gabbro dikes are the same, and their REE patterns significantly overlap, hinting that these gabbros were derived from a common mantle source.

On the N-MORB normalized incompatible trace element diagram, most of the samples have slightly negative anomalies in Nb-Ta and Ti, and a few samples also show weakly negative Zr, Hf and Th anomalies (Figs. 6c, 6d). The rocks are mostly enriched in LILE, but few samples are depleted in Pb and Sr. It can be postulated that the gabbros have similar incompatible trace element signature as suprasubduction zone basaltic rocks.

## 5.2 U-Pb Dating

One cumulate gabbro (dp1703) is selected for zircon LA-ICP-MS dating, and the analytical data are listed in Table 2. Zircons separated from this sample are weakly elongated or rounded grains or fragments of larger grains, locally with very narrow overgrowths (Fig. 7). They are mostly 100–200 µm. These zircons have relatively low U and Th concentrations (~23–238 ppm and ~14–150 ppm, respectively, Table 2), yielding Th/U ratios (0.22–0.86). These high Th/U ratios in zircons are suggestive of magmatic crystallization (Hoskin and Schaltegger 2003). Eighteen analyses of these zircons have  $^{206}\text{Pb}/^{238}\text{U}$  ages ranging from ~110 to ~120 Ma, and form a coherent group with a weighted mean of  $^{206}\text{Pb}/^{238}\text{U}$  age of  $114.3 \pm 1.4$  Ma (95% confidence; MSWD=0.72) (Fig. 8). This U-Pb date could be interpreted to represent the crystallization age of the gabbro, which is the same as that of gabbro dike (~115 Ma, unpublished data).

## 5.3 Zircon Trace Element Composition

In situ studies of the REE chemistry of these zircons

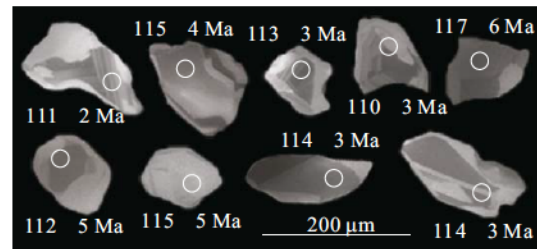


**Figure 7. Representative cathodoluminescence images of zircon grains from the cumulate gabbro.**

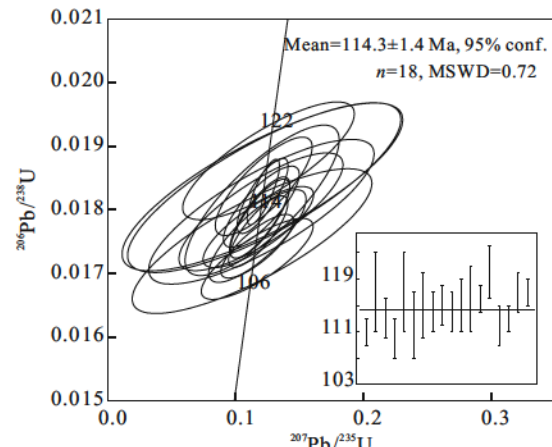


**Figure 8. U-Pb concordia diagram for zircons from the cumulate gabbro.**

**Table 2** Zircon LA-ICP-MS U-Pb data for Zhongcang cumulate gabbro

Spot No.	$^{206}\text{Pb}$ (ppm)	$^{206}\text{Pb}_{\text{bc}}$ (ppm)	U (ppm)	Th (ppm)	Th/U	$^{207}\text{Pb}/^{206}\text{Pb}$	$1\sigma$	$^{207}\text{Pb}/^{235}\text{U}$	$1\sigma$	$^{206}\text{Pb}/^{238}\text{U}$ U	$1\sigma$	$^{206}\text{Pb}/^{238}\text{U}$ age (Ma)
D1703-05	15.76	4.26	238	91	0.38	0.0487	0.0078	0.1171	0.0187	0.0174	0.0003	111±2
D1703-08	5.2	1.56	75	25	0.33	0.0484	0.0280	0.1226	0.0706	0.0184	0.0009	117±6
D1703-09	9.93	2.85	147	73	0.49	0.0482	0.0117	0.1180	0.0286	0.0177	0.0004	113±3
D1703-22	12.89	3.92	197	150	0.76	0.0493	0.0122	0.1171	0.0289	0.0172	0.0004	110±3
D1703-23	6.68	2.06	96	37	0.38	0.0479	0.0287	0.1211	0.0725	0.0184	0.0009	117±6
D1703-24	6.93	2.09	104	67	0.64	0.0468	0.0257	0.1131	0.0619	0.0175	0.0008	112±5
D1703-25	7.24	2.13	106	35	0.33	0.0486	0.0236	0.1204	0.0582	0.0180	0.0008	115±5
D1703-01	4.97	1.50	72	47	0.66	0.0483	0.0064	0.1190	0.0156	0.0179	0.0004	114±3
D1703-05	3.64	1.01	52	21	0.40	0.0483	0.0079	0.1203	0.0196	0.0181	0.0004	115±3
D1703-06	6.82	1.98	98	51	0.52	0.0484	0.0063	0.1192	0.0154	0.0179	0.0004	114±3
D1703-08	2.67	0.82	38	26	0.69	0.0485	0.0172	0.1201	0.0424	0.0180	0.0006	115±4
D1703-13	1.61	0.50	23	14	0.62	0.0483	0.0160	0.1210	0.0398	0.0182	0.0008	116±5
D1703-14	6.19	1.74	88	39	0.45	0.0483	0.0053	0.1213	0.0132	0.0182	0.0004	116±2
D1703-17	3.17	1.02	44	38	0.86	0.0486	0.0172	0.1259	0.0443	0.0188	0.0006	120±4
D1703-20	6.33	2.00	93	69	0.74	0.0483	0.0104	0.1173	0.0251	0.0176	0.0005	112±3
D1703-21	7.87	2.26	115	48	0.42	0.0484	0.0063	0.1179	0.0153	0.0177	0.0004	113±2
D1703-22	4.49	1.29	63	33	0.51	0.0482	0.0099	0.1222	0.0250	0.0184	0.0005	117±3
D1703-23	13.97	3.78	198	44	0.22	0.0483	0.0034	0.1219	0.0083	0.0183	0.0003	117±2

Note:  $^{206}\text{Pb}_{\text{bc}}$  is common lead;  $^{206}\text{Pb}$  is radiogenic lead.

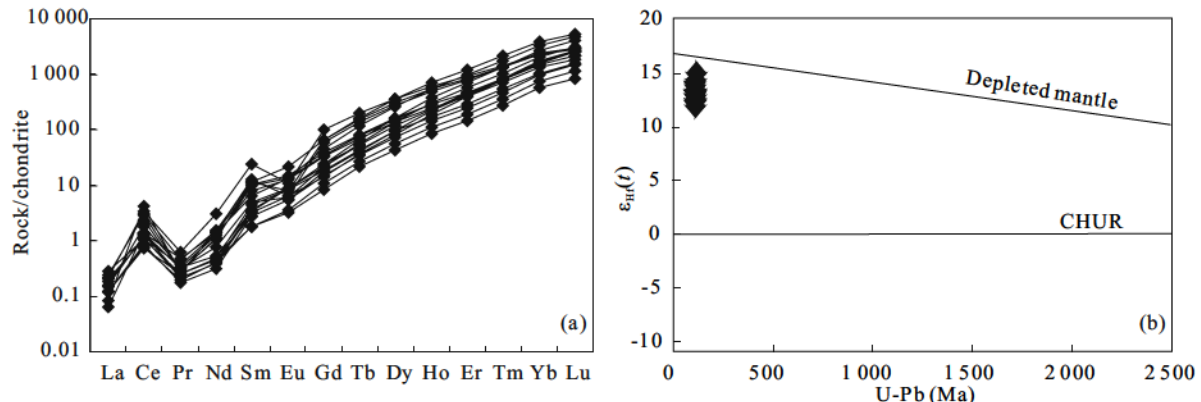


**Figure 9.** (a) Chondrite normalized REE diagrams for the zircon from cumulate gabbro (normalizing values are from Sun and McDonough, 1989). (b) Hf isotope ratio vs. Hf single stage model age of zircon from cumulate gabbro. Reference lines representing chondritic Hf evolution (CHUR) and the depleted mantle (DM) are from Blichert-Toft and Albarède (1997), Mo et al. (2009) and Griffin et al. (2000), respectively.

show it to be strongly HREE enriched with respect to the LREE, with positive Ce anomaly ( $\text{Ce}/\text{Ce}^*=4.19-27.42$ ) (Fig. 9a).

In addition, a negative Eu anomaly of variable magnitude is also observed ( $\text{Eu}/\text{Eu}^*=0.23-0.88$ ), except for four grains, which has no Eu anomaly ( $\text{Eu}/\text{Eu}^*=0.92-1.01$ ). The lack of negative Eu anomaly suggests zircon crystallization in the absence of plagioclase (Renna and Tribuzio, 2009). Cor-

rected Ti-in-zircon crystallization temperatures using the recalibrated Ti-in-zircon equation of Ferry and Watson (2007) have been calculated for the analyzed zircons (Table 3). Based on the general absence of rutile and quartz in these cumulate gabbros, implying that both  $\alpha_{\text{TiO}_2}$  and  $\alpha_{\text{SiO}_2}$  are  $\leq 1$ , we have assumed maximum  $\alpha_{\text{TiO}_2}$  and  $\alpha_{\text{SiO}_2}$  values of 1 for all samples. Using these maximum temperature estimates (Table 3), zircons

**Table 3** Zircon trace element (LA-ICP-MS) composition (in ppm), Zhongcang cumulate gabbro

Spot No.	D1703-05	D1703-08	D1703-09	D1703-22	D1703-23	D1703-24	D1703-25	D1703-01	D1703-05
Ti	7.63	5.77	7.22	10.18	7.79	6.45	6.98	4.71	5.47
Y	661	379	920	1 193	422	464	403	404	188
Zr	497 058	505 536	499 018	511 890	526 513	519 048	489 848	465 518	459 570
Nb	0.35	0.24	0.41	0.43	0.20	0.18	0.28	0.23	0.21
La	-	-	-	-	0.01	-	-	0.04	0.03
Ce	1.23	0.80	1.44	1.89	0.83	0.85	0.82	0.75	0.47
Pr	-	-	0.03	0.04	0.03	0.04	0.02	0.03	0.01
Nd	0.21	0.23	0.52	0.70	0.37	0.65	-	0.59	0.19
Sm	0.51	0.42	1.53	1.75	0.73	0.96	0.73	1.22	0.28
Eu	0.50	0.31	0.76	1.23	0.50	0.76	0.36	0.73	0.21
Gd	5.00	3.52	9.42	13.32	4.9	7.29	4.42	6.72	2.25
Tb	2.44	1.55	4.36	6.00	2.00	2.89	1.98	2.60	0.98
Dy	41.23	24.29	67.37	92.02	29.27	39.45	29.47	34.16	14.49
Ho	21.27	12.25	31.58	41.04	13.52	16.42	13.14	13.62	6.23
Er	118	68.74	164	202	72.43	76.56	75.02	64.65	32.05
Tm	34.28	20.38	44.55	53.55	20.99	20.45	21.44	17.95	9.21
Yb	454	269	567	646	275	255	299	223	129
Lu	102	63.84	120	134	62.79	55.14	67.76	45.69	28.43
Hf	5 231	5 680	6 040	5 901	5 588	5 964	6 706	5 618	5 452
Ta	0.21	0.13	0.23	0.25	0.13	0.11	0.19	0.08	0.11
Eu/Eu*	0.95	0.79	0.61	0.78	0.81	0.87	0.61	0.78	0.81
Ce/Ce*	-	-	-	-	9.63	-	-	5.30	5.13
T (°C)	724	700	719	750	726	709	716	683	695
Spot No.	D1703-06	D1703-08	D1703-13	D1703-14	D1703-17	D1703-20	D1703-21	D1703-22	D1703-23
Ti	5.69	12.26	16.03	4.95	18.39	4.63	6.63	5.78	5.16
Y	142	860	802	238	987	476	546	294	343
Zr	462 385	458 051	464 054	463 401	472 153	474 775	485 874	498 257	469 828
Nb	0.20	0.26	0.47	0.30	0.28	0.24	0.31	0.27	0.32
La	0.03	0.06	0.02	0.03	0.05	0.07	0.04	0.05	0.04
Ce	0.45	1.79	2.5	0.53	2.11	0.65	1.08	0.65	0.67
Pr	0.02	0.03	0.02	0.02	0.06	0.03	0.03	0.02	0.02
Nd	0.21	0.50	0.69	0.15	1.41	0.63	0.25	0.22	0.18
Sm	0.27	1.79	1.94	0.42	3.58	1.56	0.54	0.68	0.49
Eu	0.19	0.46	0.37	0.32	0.63	0.85	0.51	0.49	0.37
Gd	1.71	13.23	11.91	3.08	20.26	8.12	4.39	3.86	2.87
Tb	0.79	5.78	5.22	1.28	7.51	3.10	2.14	1.62	1.35
Dy	11.03	75.55	68.58	18.22	92.43	40.07	34.71	23.47	20.35
Ho	4.78	30.90	28.19	8.15	34.65	16.69	17.05	9.84	10.65
Er	24.33	141	130	41.25	152	76.99	93.59	48.34	64.28
Tm	7.12	34.80	34.36	11.93	36.88	20.60	26.56	14.01	20.57
Yb	96.66	396	388	168	405	259	353	175	295
Lu	20.76	72.09	74.83	37.58	73.94	54.48	78.87	38.98	68.83
Hf	6 387	8 746	8 328	5 284	8 418	5 765	5 313	5 553	5 351
Ta	0.07	0.19	0.31	0.11	0.20	0.10	0.15	0.05	0.14
Eu/Eu*	0.84	0.29	0.24	0.88	0.23	0.73	1.01	0.92	0.95
Ce/Ce*	4.27	11.0	27.9	6.10	9.52	3.38	7.90	4.73	5.53
T (°C)	699	768	794	687	808	682	712	700	690

Note: Eu/Eu\*=Eu<sub>N</sub>/SQRT(Sm<sub>N</sub>×Gd<sub>N</sub>); Ce/Ce\*=Ce<sub>N</sub>/SQRT(La<sub>N</sub>×Pr<sub>N</sub>); T after Ferry and Watson (2007) using  $\alpha_{\text{SiO}_2}=1$ ,  $\alpha_{\text{TiO}_2}=1$ .

from Zhongcang cumulate gabbros give a T range of 681–808 °C, similar to that of mafic rocks from the mid-ocean

ridges studied by Grimes et al. (2009).

#### 5.4 Zircon Lu-Hf Isotopes

Of the 18 dated zircons from cumulate gabbro, 17 were analyzed for Hf isotope ratios. These zircons show a wide range of  $^{176}\text{Lu}/^{177}\text{Hf}$  ratios (0.000 583–0.002 320) and  $^{176}\text{Yb}/^{177}\text{Hf}$  (0.018 460–0.077 769) (Table 4). However, they

give a narrow range of initial  $^{176}\text{Hf}/^{177}\text{Hf}$  from 0.283 041 to 0.283 123. All zircons have positive  $\epsilon_{\text{Hf}}(t)$  values ranging from +11.9 to +15.0. The single stage Hf model ages (TDM) calculated is 181–302 Ma (Table 4).

**Table 4** Hf isotopic compositions for zircon of Zhongcang cumulate gabbro

Spot No.	$^{176}\text{Hf}/^{177}\text{Hf}$	$1\sigma$	$^{176}\text{Lu}/^{177}\text{Hf}$	$1\sigma$	$^{176}\text{Yb}/^{177}\text{Hf}$	$1\sigma$	Age (Ma)	$\epsilon_{\text{Hf}}(t)$	$1\sigma$	$T_{\text{DM1}}$ (Ma)	$T_{\text{DM2}}$ (Ma)
D1703-05	0.283 057	0.000 018	0.000 843	0.000 021	0.026 484	0.000 784	114	12.5	0.8	275	339
D1703-08	0.283 108	0.000 010	0.001 919	0.000 041	0.065 081	0.001 077	111	14.2	0.6	208	243
D1703-09	0.283 075	0.000 010	0.000 850	0.000 017	0.023 638	0.000 258	117	13.2	0.6	249	302
D1703-22	0.283 082	0.000 012	0.002 320	0.000 024	0.077 769	0.000 591	113	13.3	0.7	249	296
D1703-23	0.283 082	0.000 011	0.000 583	0.000 014	0.018 460	0.000 287	110	13.3	0.6	238	290
D1703-24	0.283 066	0.000 008	0.001 336	0.000 078	0.043 332	0.002 490	117	12.9	0.6	265	322
D1703-25	0.283 054	0.000 007	0.000 956	0.000 012	0.038 106	0.000 203	112	12.3	0.6	280	347
D1703-01	0.283 082	0.000 014	0.001 625	0.000 046	0.054 434	0.001 449	115	13.4	0.7	244	292
D1703-05	0.283 041	0.000 010	0.001 572	0.000 052	0.050 412	0.001 574	115	11.9	0.6	302	372
D1703-06	0.283 094	0.000 011	0.000 912	0.000 028	0.028 847	0.001 105	114	13.8	0.6	223	266
D1703-08	0.283 057	0.000 012	0.000 972	0.000 022	0.031 711	0.000 601	115	12.5	0.7	275	338
D1703-13	0.283 107	0.000 010	0.000 719	0.000 023	0.022 859	0.000 905	116	14.4	0.6	202	237
D1703-14	0.283 082	0.000 007	0.000 821	0.000 005	0.032 811	0.000 330	116	13.4	0.6	240	289
D1703-17	0.283 123	0.000 059	0.001 065	0.000 045	0.034 797	0.001 379	120	15.0	2.2	182	206
D1703-20	0.283 073	0.000 009	0.001 326	0.000 009	0.052 010	0.000 315	112	13.0	0.6	255	309
D1703-21	0.283 100	0.000 011	0.000 631	0.000 012	0.021 197	0.000 454	113	14.1	0.7	212	252
D1703-23	0.283 054	0.000 012	0.002 080	0.000 032	0.065 666	0.000 680	117	12.4	0.7	289	349

## 6 DISCUSSION

### 6.1 Petrogenesis of the Gabbros

Immobile elements, such as Zr, Nb and Yb, are employed to discriminate the nature of the magma source, and their ratios (e.g., Nb/Yb) can provide a robust indicator of mantle fertility (e.g., Pearce and Stern, 2006). The Nb/Yb ratios of Zhongcang gabbros are in range of 0.39–1.60, most of which are higher than that of N-MORB (0.76, Sun and McDonough, 1989), but lower than that of E-MORB (3.5, Sun and McDonough, 1989), indicating that the mantle source of these rocks is probably a mixture of enriched mantle and depleted mantle. The  $\epsilon_{\text{Hf}}(t)$  values (+11.9 to +15.0) of zircons from cumulate gabbro are slightly below depleted mantle values (Fig. 9b), also suggesting the involvement of enriched mantle components on the origin of these Zhongcang gabbros. The enriched mantle is generally thought to be related to recycling of subducted crust (Donnelly et al., 2004). Pearce and Parkinson (1993) compiled bulk distribution coefficients for highly incompatible to compatible elements of mantle derivation (e.g., Nb, Yb, Y), and showed characteristic of basalts from different tectonic settings by normalizing primitive basalts against a fertile MORB mantle (FMM). We have applied this method to the gabbros of Zhongcang ophiolitic mélangé as shown in Figs. 10a and b, and the cumulate gabbros and gabbro dikes show the similar FMM-normalized patterns. Typically, the patterns of the cumulate gabbros and gabbro dikes have the following incompatible element characteristics: VHI>HI>MI or VHI≥HI=MI (Figs.

10a, 10b). According to Pearce and Parkinson (1993), such patterns indicate moderate to high degrees of melting of an un-enriched to slightly depleted FMM source. The gabbros have uniformly low Dy/Yb ratios (1.66–1.82) and relatively elevated La/Yb ratios (0.75–1.71) (Table 1), and plot within the melting trend of spinel mantle source, which corresponds to ~30% partial melting of a spinel Iherzolite mantle (Fig. 11a). Sm/Yb and La/Sm ratios are employed to further constrain the nature of the spinel mantle (Fig. 11b).

As mentioned above, Zhongcang gabbros show clear LILE enrichments caused by the mobility of LILE in fluids or melts from the subducting oceanic crust and sediments (e.g., Pearce and Stern, 2006 and references therein; Pearce and Peate, 1995). High Sr/Nd ratios are generally attributed to the involvement of slab-derived fluids, whereas high Th/Yb ratios have been ascribed to the addition of subducted sediments (Davidson, 1987). In Zhongcang gabbros, Sr/Nd ratio is 10.45–73.31, higher than that of N-MORB (12.33, Sun and McDonough, 1989) and upper crust (11.85, Rudnick and Gao, 2003). The Th/Yb ratio is in range of 0.02–0.36, similar to that of N-MORB (0.04, Sun and McDonough, 1989) and E-MORB (0.25, Sun and McDonough, 1989). These suggest the lack of a sediment component in generation of the gabbros. Pearce (2008) proposed that fluids released from subducted material and their interaction with mantle sources will result in high U/Th and Ba/Th in produced magmas. At low Th concentrations, some gabbro dikes show a large spread in U/Th and Ba/Th

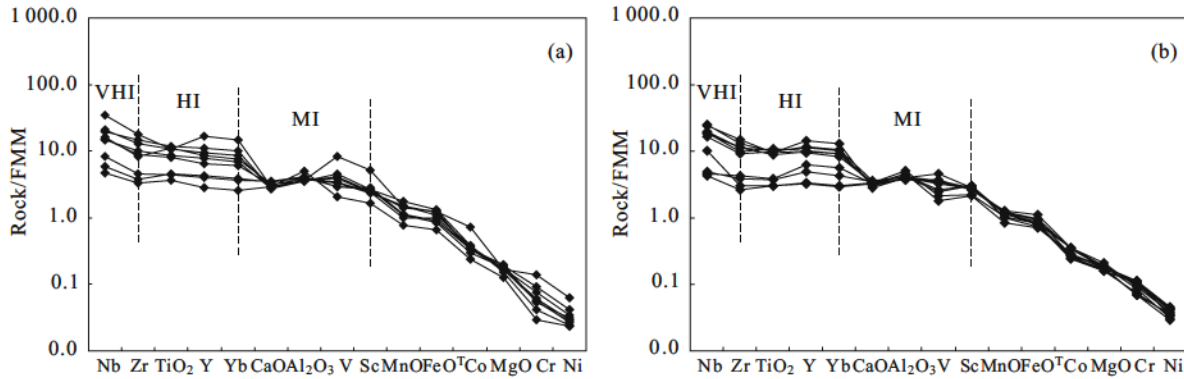


**Figure 10.** FMM (fertile MORB mantle) normalized patterns for cumulate gabbro (a) and gabbro dike (b) (normalizing values are from Pearce and Parkinson, 1993). VHI. Very highly incompatible element; HI. highly incompatible element; MI. moderately incompatible element.

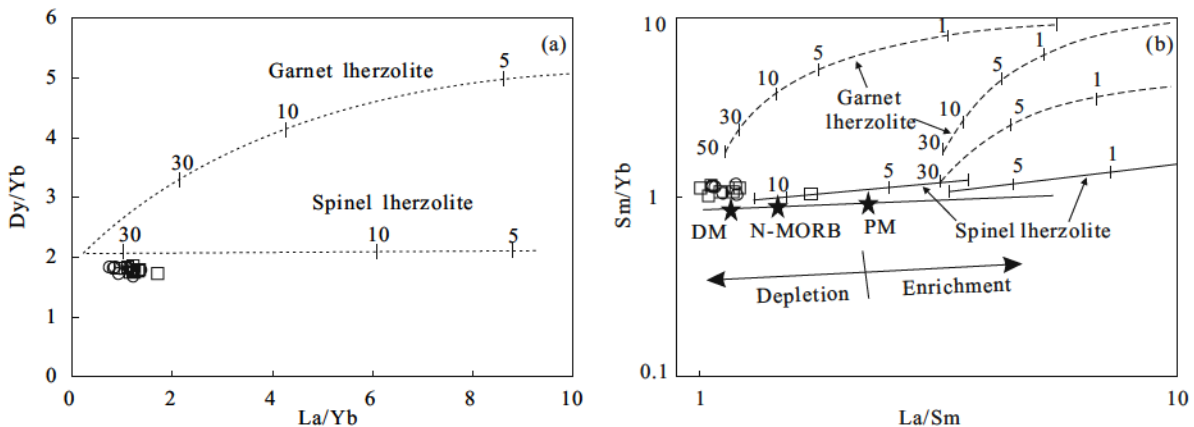


**Figure 11.** (a) Dy/Yb vs. La/Yb diagram (after Xu et al., 2001). (b) Sm/Yb vs. La/Sm diagram (after Zhao and Zhou, 2007). Mantle array (heavy line) defined by depleted MORB mantle (DMM, McKenzie and O’Nions, 1991) and primitive mantle (PM, Sun and McDonough, 1989). Melting curves for spinel lherzolite and garnet peridotite with both DMM and PM compositions are after Aldanmaz et al. (2000). Numbers along lines represent the degree of the partial melting. The legend is shown in Fig. 4.

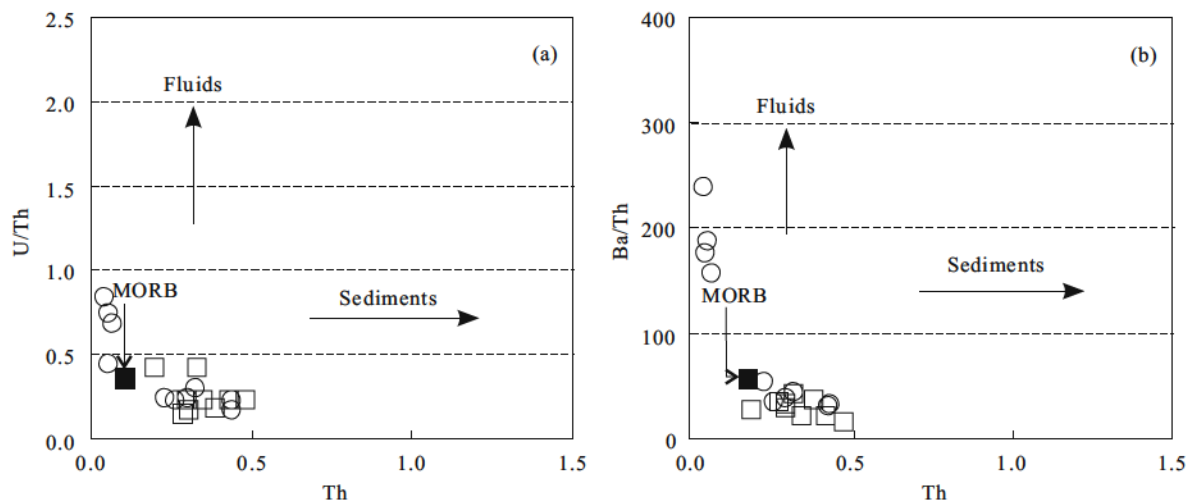


**Figure 12.** U/Th (a) and Ba/Th (b) vs. Th diagrams showing the subduction effect upon gabbros of Zhongcang ophiolitic mélange (after Dilek et al., 2008). The legend is shown in Fig. 4.

(Figs. 12a and 12b), suggesting that they were generated from a mantle source that was enriched in Ba and U, as well as in other fluid-mobilized elements. In contrary, the other gabbro dikes

and cumulate gabbros have slightly higher Th contents than MORB, indicating that they were derived from a source that has been enriched in Th by melts derived from subducted se-

diments (Figs. 12a and 12b). In summary, the mantle source of these gabbros was probably enriched by interaction with slab-derived fluids and melts from sediment.

## 6.2 Tectonic Setting

The hybrid mixture between MORB-like and arc-like element signatures in Zhongcang gabbros is generally acknowledged to be unique to backarc basin basalt (Pearce and Stern, 2006; Pearce and Peate, 1995; Volpe et al., 1987). In addition, these gabbros of Zhongcang ophiolitic mélange mainly plot in the back-arc basin basalt field and between volcanic arc and N-MORB fields on the triangular Y-La-Nb diagram (Fig. 13a). On Ti verse V diagram, all of the gabbros show similarities to MORB and island arc tholeiites (IAT) (Fig. 13b). These characteristics suggest that Zhongcang ophiolitic mélange were probably formed in a back arc setting with strong MORB related characteristics.

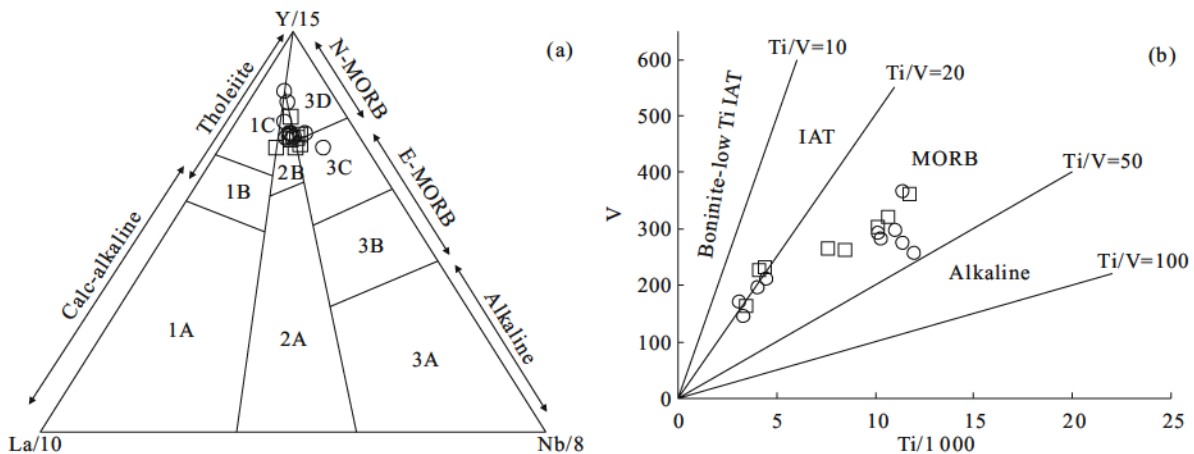


**Figure 13.** (a) Triangular Y/15-La/10-Nb/8 diagram of Cabanis and Lecolle (1989). 1A. Calc-alkaline basalts; 1B. overlap between 1A and 1C; 1C. volcanic arc tholeiites; 2A. continental basalts; 2B. backarc basin basalts; 3A. alkaline basalts; 3B and 3C. E-MORB; 3D. N-MORB. (b) Ti (ppm) versus V (ppm) diagram for the gabbros from Zhongcang ophiolitic mélange. Ti/V ratios for IAT and MORB are from Shervais (1982). The legend is shown in Fig. 4.

## 6.3 Implications for the Evolution of the Neo-Tethys in Central Tibet

The new geochemical data and LA-ICP-MS U-Pb age dates show that Zhongcang ophiolitic mélange was formed in an intra-oceanic back arc basin in Early Cretaceous. Previous studies suggested that Shiquanhe ophiolitic mélange in the western part of SYJMB was derived from a subduction-related environment (Qiu et al., 2005; Xu et al., 2004), and the formation age is Middle Jurassic (Fig. 15; Zheng et al., 2006). The Guchang ophiolitic mélange is believed to have started building during Jurassic and lasted to Early Cretaceous, representing for a limited oceanic basin (Chen et al., 2006). Zeng et al. (2006) and Wang et al. (2007) concluded that Lagkorco ophiolitic mélange was generated in an inter-arc basin setting. However, the amphibolites show greater arc affinity similar to basalts from back-arc basin settings (Wang et al., 2008).

The isotope dating and radiolarian show an age range of later Early Jurassic and Early Cretaceous (Fig. 15; Fan et al., 2010; Zhang et al., 2007; Aitchison and Davis, 2006; Zeng et al., 2006). A K-Ar age of  $118.74 \pm 4.75$  Ma and Early Cretaceous radiolarian are reported in Asuo structure mélange, which

Previous studies have shown that back-arc basin basalts may form not only on an intra-oceanic arc lithosphere such as Mariana Trough (Gribble et al., 1996), but also on a continental basement such as the Okinawa Trough (Shinjo et al., 1999). Generally, intra-oceanic back arc basin basalts are similar to N-MORB to intra-oceanic arc magmas, whereas compositions of continental back-arc basin basalts are similar to E-MORB to continental arc magmas (Ghazi et al., 2012). The chondrite normalized REE patterns of Zhongcang gabbros are similar to N-MORB (Figs. 6a and 6b). Most of Zhongcang gabbros plot in the MORB array close to N-MORB on some of the diagnostic HFSE and REE ratio diagram, and some cumulate gabbros plot between the MORB array and compositional field for typical arc basalts (Fig. 14). These observations propose that the Zhongcang gabbros most likely are related to an oceanic back arc and oceanic arc setting.

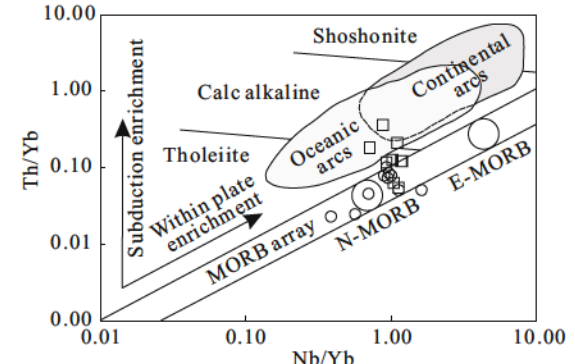


**Figure 14.** Th/Yb versus Nb/Yb diagram for gabbros (after Pearce and Peate, 1995).

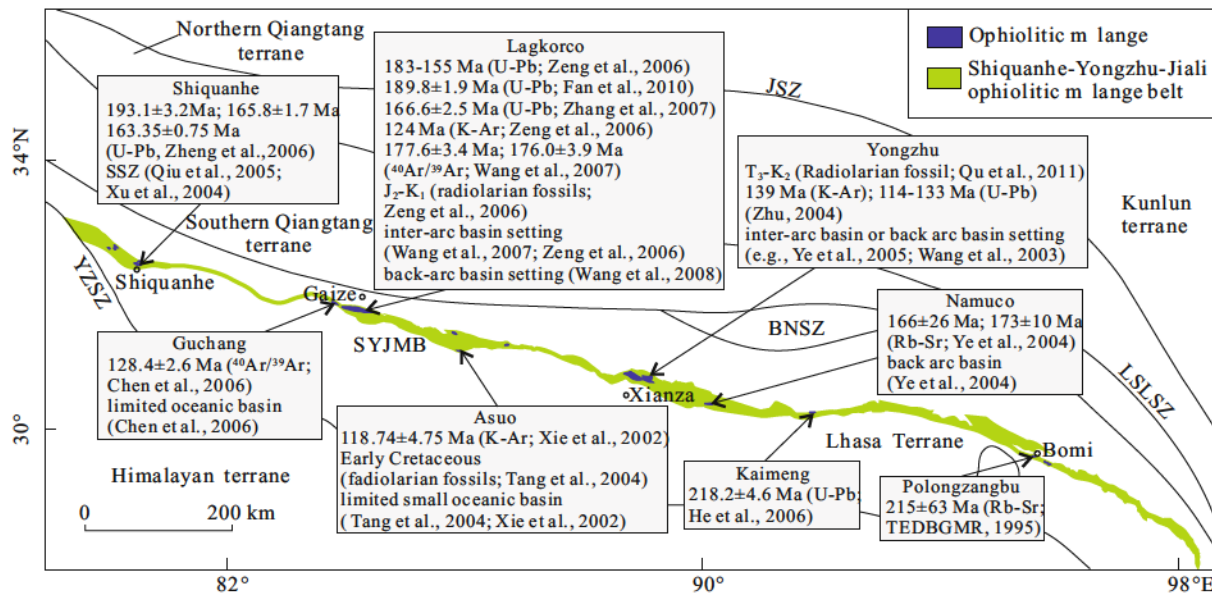


**Figure 15.** A summary of the recent geochronologic and geotectonic data on the SYJMB, showing the ages and the tectonic settings of the various ophiolitic mélanges (see text for details and references). SSZ. Supra-subduction zone; Map legend is presented in Fig. 1.

The K-Ar and U-Pb techniques provided Early Cretaceous ages for Yongzhu ophiolitic mélange (Zhu, 2004; Wang et al., 2003), but radiolarites yielded ages spanning from Late Triassic to Late Cretaceous (Fig. 15; Qu et al., 2011; Wang et al., 2003). The geochemistry of mafic rocks shows that the Namuco ophiolite mélange derived from the dismantlement of back arc basin system of Middle Jurassic (Ye et al., 2004). The Kaimeng and Polongzangbu ophiolitic mélanges was both considered to form in a suprasubduction zone system (He et al., 2006; Zheng et al., 2003). Although some Late Triassic–Early Jurassic ages have been reported in Shiquanhe, Kaimeng and Polongzangbu ophiolitic mélanges, no related geochemical data can be used to investigate their tectonic setting. All of these observations suggest that SYJMB probably represents an intra-oceanic back arc basin during the Middle Jurassic and Early Cretaceous.

Between SYJMB and BNSZ, a large magmatic arc is oriented in an E-W direction, which mainly includes Middle–Late Jurassic and Early Cretaceous volcanic rocks with island arc affinities and I-typed granites (Zhu et al., 2011, 2008; Pan et al., 2006). The Lu-Hf isotope characteristics of zircons from these magmatic rocks show that they are derived from mantle source, implying that the northern subterrane is recently accreted (Zhu et al., 2011). In addition, Qiu et al. (2004) and Shi (2007) reported 152.3±3.6 and 167.0±1.4 Ma for Shemalgou ophiolite and Bangonghu ophiolite, respectively, and they interpreted these ages as the subduction of the BNSZ. These propose that an intra-oceanic southward subduction system was probably developed in Neo-Tethy Ocean in central Tibet during the Middle Jurassic and Early Cretaceous (Zhu et al., 2011, 2008).

In summary, the Neo-Tethy Ocean in central Tibet has been probably subducted southward in Middle Jurassic and led to the generation of an inter-oceanic island arc. Then an intra-oceanic back arc basin was formed and lasted to Early Cretaceous.

## 7 CONCLUSION

The Zhongcang ophiolitic mélange is dominated by cumulate gabbros, gabbro dikes and metamorphic peridotite, with minor volcanic rocks. The gabbros have undergone greenschist-amphibolite facies metamorphism. The whole rock geochemistry indicates that these gabbros were derived from a common mantle source, and have MORB and volcanic arc affinities. The mantle source of the gabbros in Zhongcang ophiolitic mélange was spinel mantle with ~30% partial melting, and was enriched by slab-derived fluids and melts from sediment. This study suggests that the Zhongcang ophiolitic mélange was formed in an intra-oceanic back arc system in Early Cretaceous.

Comparable observations from the other ophiolitic massifs along the whole Shiquanhe-Yongzhu-Jiali ophiolitic mélange belt and the ages of magmatic arc and BNSZ subduction allow us to propose that an intra-oceanic subduction system and back arc basin operated in the Neo-Tethy Ocean of central Tibet during Middle Jurassic and Early Cretaceous, resembling modern active intra-oceanic subduction systems in the western Pacific.

## ACKNOWLEDGMENTS

We appreciate Prof. Yongsheng Dong for his help during petrography work. We thank research team of Tibet, Jilin University for their assistance with the fieldwork and Profs. Li Su, Jiao Li and Hongyu Zhang for their assistance with geochemical analysis and zircon U-Pb dating. We also thank reviewers for their comments. This research was supported by the National Nature Science Foundation of China (No. 41272240) and the Project of China Geological Survey (No. 1212011121248).

## REFERENCES CITED

- Aitchison, J. C., Davis, A. M., 2006. The Nature and Age of

- Oceanic Rocks along the Bangong-Nujiang Suture Zone in Central Tibet. *Journal of Asian Earth Sciences*, 26: 123
- Aldanmaz, E., Pearce, J. A., Thirlwall, M. F., et al., 2000. Petrogenetic Evolution of Late Cenozoic, Post-Collision Volcanism in Western Anatolia, Turkey. *Journal of Volcanology and Geothermal Research*, 102: 67–95
- Andersen, T., 2002. Correction of Common Lead in U-Pb Analyses that do not Report  $^{204}\text{Pb}$ . *Chemical Geology*, 192: 59–79
- Blichert-Toft, J., Albarède, F., 1997. The Lu-Hf Isotope Geochemistry of Chondrites and the Evolution of the Mantle-Crust System. *Earth and Planetary Science Letters*, 148: 243–258
- Cabanis, B., Lecolle, M., 1989. The La/10-Y/15-Nb/8 Diagram: A Tool for Discrimination Volcanic Series and Evidencing Continental Crust Magmatic Mixtures and/or Contamination. *Compte Rendu de l'Academie des Sciences, Series II, Mécanique, Physique, Chimie, Sciences de l'univers, Sciences de la Terre*, 309(20): 2023–2029 (in French)
- Chen, Y. L., Zhang, K. Z., Gou, Y. D., et al., 2006. 1 : 250 000 Geological Report of Wuma. Unpublished (in Chinese)
- Coward, M. P., Kidd, W. S. F., Yun, P., et al., 1988. The Structure of the 1985 Tibet Geotraverse, Lhasa to Golmud. *Philosophical Transactions of the Royal Society of London, Series A*, 327: 307–336
- Davidson, J. P., 1987. Crustal Contamination versus Subduction Zone Enrichment: Examples from the Lesser Antilles and Implications for Mantle Source Compositions of Island Arc Volcanic Rocks. *Geochimica et Cosmochimica Acta*, 51: 2185–2198
- Dewey, J. F., Shackleton, R. M., Chengfa, C., et al., 1988. The Tectonic Evolution of the Tibetan Plateau. *Philosophical Transactions of the Royal Society of London Series A*, 327: 379–413
- Dilek, Y., Furnes, H., Shallo, M., 2008. Geochemistry of the Jurassic Mirdita Ophiolite (Albania) and the MORB to SSZ Evolution of a Marginal Basin Oceanic Crust. *Lithos*, 100: 174–209
- Donnelly, K. E., Goldstein, S. L., Langmuir, C. H., et al., 2004. Origin of Enriched Ocean Ridge Basalts and Implications for Mantle Dynamics. *Earth and Planetary Science Letters*, 226: 347–366
- Fan, S. Q., Shi, R. D., Ding, L., et al., 2010. Geochemical Characteristics and Zircon U-Pb Age of the Plagiogranite in Gaize Ophiolite of Central Tibet and Their Tectonic Significance. *Acta Petrologica et Mineralogica*, 29(5): 467–478 (in Chinese with English Abstract)
- Ferry, J. M., Watson, E. B., 2007. New Thermodynamic Models and Revised Calibrations for the Ti-in-Zircon and Zr-in-Rutile Thermometers. *Contributions to Mineralogy and Petrology*, 154: 429–437, doi:10.1007/s00410-007-0201-0
- Geng, Q. R., Pan, G. T., Wang, L. Q., et al., 2011. Tethyan Evolution and Metallogenic Geological Background of the Bangong Co-Nujiang Belt and the Qiangtang Massif in Tibet. *Geological Bulletin of China*, 30: 1261–1274 (in Chinese with English Abstract)
- Ghazi, J. M., Moazzen, M., Rahgoshay, M., et al., 2012. Geochemical Characteristics of Basaltic Rocks from the Nain Ophiolite (Central Iran): Constraints on Mantle Wedge Source Evolution in an Oceanic Back Arc Basin and a Geodynamical Model. *Tectonophysics*, 574–575: 92–104
- Girardeau, J., Marcoux, J., Allegre, C. J., et al., 1984. Tectonic Environment and Geodynamic Significance of the Neo-Cimmerian Donqiao Ophiolite, Bangong-Nujiang Suture Zone, Tibet. *Nature*, 307: 27–31
- Girardeau, J., Marcoux, J., Fourcade, E., et al., 1985. Xainxa Ultramafic Rocks, Central Tibet, China: Tectonic Environment and Geodynamic Significance. *Geology*, 13: 330–333
- Gribble, R. F., Stern, R. J., Bloomer, S. H., et al., 1996. MORB Mantle and Subduction Components Interact to Generate Basalts In the Southern Mariana Trough Backarc Basin. *Geochimica et Cosmochimica Acta*, 60(12): 2153–2166
- Griffin, W. L., Pearson, N. J., Belousova, E., et al., 2000. The Hf Isotope Composition of Cratonic Mantle: LAM-MC-ICPMS Analysis of Zircon Megacrysts in Kimberlites. *Geochimica et Cosmochimica Acta*, 64(1): 133–147
- Grimes, C., John, B., Cheadle, M., et al., 2009. On the Occurrence, Trace Element Geochemistry, and Crystallization History of Zircon from In Situ Ocean Lithosphere. *Contributions to Mineralogy and Petrology*, 158: 757–783, doi:10.1007/s00410-009-0409-2
- He, Z. H., Yang, D. M., Wang, T. W., 2006. Age, Geochemistry and Its Tectonic Significance of Kaimeng Ophiolites in Jiali Fault Belt, Tibet. *Acta Petrologica Sinica*, 22: 653–660 (in Chinese with English Abstract)
- Hoskin, P. W. O., Schaltegger, U., 2003. The Composition of Zircon and Igneous and Metamorphic Petrogenesis. *Reviews in Mineralogy and Geochemistry*, 53(1): 27–62
- Hu, C., 1990. Characteristics of Shiquanhe-Guchang Ophiolite Belt and Its Geologic Significance. *Journal of Chengdu College of Geology*, 17: 23–30 (in Chinese with English Abstract)
- Hu, Z., Liu, Y., Gao, S., et al., 2012. Improved In Situ Hf Isotope Ratio Analysis of Zircon Using Newly Designed X Skimmer Cone and Jet Sample Cone in Combination with the Addition of Nitrogen By Laser Ablation Multiple Collector ICP-MS. *Journal of Analytical Atomic Spectrometry*, 27: 1391–1399
- Kakar, M. I., Mahmood, K., Khan, M., et al., 2013. Petrology and Geochemistry of Gabbros from the Muslim Bagh Ophiolite: Implications for Their Petrogenesis and Tectonic Setting. *Journal of Himalayan Earth Sciences*, 46(1): 19–30
- Kapp, P., Murphy, M. A., Yin, A., et al., 2003. Mesozoic and Cenozoic Tectonic Evolution of the Shiquanhe Area of Western Tibet. *Tectonics*, 22(4): 1029, doi:10.1029/2001TC001332
- Li, C., 1987. The Longmucuo-Shuanghu-Langcangjiang Plate Suture and the North Boundary of Distribution of Gondwana Facies Permo-Carboniferous System in Northern Xizang, China. *Journal of Changchun College of*

- Geology*, 17(2): 155–166 (in Chinese with English Abstract)
- Li, C., Zhai, Q. G., Dong, Y. S., et al., 2009. High-Pressure Eclogite-Blueschist Metamorphic Belt and Closure of Paleo-Tethys Ocean in Central Qiangtang, Qinghai-Tibet Plateau. *Journal of Earth Science*, 20(2): 209–218, doi:10.1007/s12583-009-0021-4
- Liu, D. Z., Tao, X. F., Ma, R. Z., et al., 2003. 1 : 250 000 Geological Report of Cuoqin County. Unpublished (in Chinese)
- Liu, Y., Wang, X., Wang, D., et al., 2012. Triassic High-Mg Adakitic Andesites from Linxi, Inner Mongolia: Insights into the Fate of the Paleo-Asian Ocean Crust and Fossil Slab-Derived Melt-Peridotite Interaction. *Chemical Geology*, 328: 89–108
- Ludwig, K. R., 2000. ISOPLOT/Ex, Version 2.2, a Geochronological Toolkit for Microsoft Excel. Berkeley Geochronological Center Special Publication, Berkeley. 1–71
- Mattern, F., Schneider, W., 2000. Suturing of the Proto- and Paleo-Tethys Oceans in the Western Kunlun (Xinjiang, China). *Journal of Asian Earth Sciences*, 18: 637–650
- McKenzie, D., O’nions, R. K., 1991. Partial Melt Distributions from Inversion of Rare Earth Element Concentrations. *Journal of Petrology*, 32: 1021–1091
- Miyashiro, A., 1974. Volcanic Rock Series in Island Arcs and Active Continental Margins. *American Journal of Science*, 274: 321–355
- Mo, X. X., Dong, G. C., Zhao, Z. D., et al., 2009. Mantle Input to the Crust in Southern Gangdese, Tibet, during the Cenozoic: Zircon Hf Isotopic Evidence. *Journal of Earth Science*, 20(2): 241–249, doi:10.1007/s12583-009-0023-2
- Pan, G. T., Ding, J., Yao, D. S., et al., 2004. Guidebook of 1:1 500 000 Geologic Map of the Qinghai-Xizang (Tibet) Plateau and Adjacent Areas. Cartographic Publishing House, Chengdu (in Chinese)
- Pan, G. T., Mo, X. X., Hou, Z. Q., et al., 2006. Spatial-Temporal Framework of the Gangdese Orogenic Belt and Its Evolution. *Acta Petrologica Sinica*, 22(3): 521 (in Chinese with English Abstract)
- Pan, G. T., Wang, L. Q., Li, R. S., et al., 2012. Tectonic Evolution of the Qinghai-Tibet Plateau. *Journal of Asian Earth Sciences*, 53: 3–14
- Pearce, J. A., 2008. Geochemical Fingerprinting of Oceanic Basalts with Applications to Ophiolite Classification and the Search for Archean Oceanic Crust. *Lithos*, 100(1–4): 14–48
- Pearce, J. A., Parkinson, I. J., 1993. Trace Element Models for Mantle Melting: Application to Volcanic Arc Petrogenesis. *Geological Society, London, Special Publications*, 76: 373–403, doi:10.1144/GSL.SP.1993.076.01.19
- Pearce, J. A., Peate, D. W., 1995. Tectonic Implications of the Composition of Volcanic ARC Magmas. *Annual Review of Earth and Planetary Sciences*, 23: 251–285
- Pearce, J. A., Stern, R. J., 2006. Origin of Backarc Basin Magmas: Trace Element and Isotope Perspectives. In: Christie, D. M., Fisher, C. R., Lee, S. M., et al., eds., Backarc Spreading Systems: Geological, Biological, Chemical, and Physical Interactions, Geophysical Monograph Series. *American Geophysical Union, Washington, D. C.*, 166: 63–86, doi:10.1029/166GM06
- Qiu, R. Z., Deng, J. F., Zhou, S., et al., 2005. Ophiolite Types in Western Qinghai-Tibetan Plateau—Evidences from Petrology and Geochemistry. *Earth Science Frontiers*, 12: 277–291 (in Chinese with English Abstract)
- Qiu, R. Z., Zhou, S., Deng, J. F., et al., 2004. Dating of Gabbro in the Shemalagou Ophiolite in the Western Segment of the BangongCo-Nujiang Ophiolite Belt, Tibet—with a Discussion of the Age of the Bangong Co-Nujiang Ophiolite Belt. *Geology in China*, 31(3): 262–268 (in Chinese with English Abstract)
- Qu, Y. G., Wang, Y. S., Duan, J. X., et al., 2011. 1 : 250 000 Geological Report of Duoba Area. China Unisversity of Geoscience Press, Wuhan (in Chinese)
- Ray, D., Misra, S., Banerjee, R., et al., 2011. Geochemical Implications of Gabbro from the Slow-Spreading Northern Central Indian Ocean Ridge, Indian Ocean. *Geological Magazine*, 148(3): 404–422
- Renna, M., Tribuzio, R., 2009. Petrology, Geochemistry and U-Pb Zircon Geochronology of Lower Crust Pyroxenites from Northern Apennine (Italy): Insights into the Post-Collisional Variscan Evolution. *Contributions to Mineralogy and Petrology*, 157: 813–835, doi:10.1007/s00410-008-0366-1
- Rudnick, R. L., Gao, S., 2003. Composition of the Continental Crust, In: Heinrich, D. H., Karl, K. T., eds., Treatise on Geochemistry. Oxford, Pergamon. 3: 1–64
- Shervais, J. W., 1982. Ti-V plots and the Petrogenesis of Modern and Ophiolitic Lavas. *Earth and Planetary Science Letters*, 59: 101–118
- Shi, R. D., 2007. SHRIMP Dating of the Bangong Lake SSZ-Type Ophiolite: Constraints on the Closure Time of the Ocean in the Bangong Lake-Nujiang River, Northwestern Tibet. *Chinese Science Bulletin*, 52(7): 936–941
- Shinjo, R., Chung, S. L., Kato, Y., et al., 1999. Geochemical and Sr-Nd Isotopic Characteristics of Volcanic Rocks from the Okinawa Trough and Ryukyu Arc: Implications for the Evolution of a Young, Intracontinental Backarc Basin. *Journal of Geophysical Research: Solid Earth*, 104(B5): 10591–10608
- Savov, I., Ryan, J., Haydoutov, I., et al., 2001. Late Precambrian Balkan-Carpathian Ophiolite—A Slice of the Pan-African Ocean Crust? Geochemical and Tectonic Insights from the Tcherni Vrah and Deli Jovan Massifs, Bulgaria and Serbia. *Journal of Volcanology and Geothermal Research*, 110: 299–318
- Scoates, J. S., 2000. The Plagioclase Magma Density Paradox Re-Examined and the Crystallization of Proterozoic Anorthosites. *Journal of Petrology*, 41(5): 627–649
- Sun, S. S., McDonough, W. F., 1989. Chemical and Isotopic Systematics of Oceanic Basalts: Implications for Mantle Composition and Processes. *Geological Society, London, Special Publications*, 42: 313–345, doi:10.1144/GSL.SP.1989.042.01.19
- Tang, L. F., Huang, J. C., Luo, X. C., et al., 2004. The

- Discovery and Significance of the Asuo Structural Mélanges in North Tibet. *Journal of East China Institute of Technology*, 27: 245–250 (in Chinese with English Abstract)
- Tibet Exploration and Development Bureau of Geology and Mineral Resources (TEDBGMR), 1995. 1 : 200 000 Geological Report of Bomi. Unpublished (in Chinese)
- Volpe, A. M., Macdougall, J. D., Hawkins, J. W., 1987. Mariana Trough basalts (MTB): Trace Element and Sr-Nd Isotopic Evidence for Mixing between MORB-Like and Arc-Like Melts. *Earth and Planetary Science Letters*, 82: 241–254
- Wang, B. D., Xu, J. F., Zeng, Q. G., et al., 2007. Geochemistry and Genesis of Lhaguo Tso Ophiolite in South of Gerze Area, Center Tibet. *Acta Petrologica Sinica*, 23: 1521–1530 (in Chinese with English Abstract)
- Wang, W. L., Aitchison, J. C., Lo, C. H., et al., 2008. Geochemistry and Geochronology of the Amphibolite Blocks in Ophiolitic Mélanges along Bangong-Nujiang Suture, Central Tibet. *Journal of Asian Earth Sciences*, 33: 122–138
- Wang, Y. S., Qu, Y. G., Lü, P., et al., 2003. The Geologic Features of Ophiolite Zone in the Yongzhu Area, Tibet. *Jilin Geology*, 22(2): 1–14 (in Chinese with English Abstract)
- Winchester, J. A., Floyd, P. A., 1977. Geochemical Discrimination of Different Magma Series and Their Differentiation Products Using Immobile Elements. *Chemical Geology*, 20: 325–343
- Xie, G. G., Zhou, A. J., Yuan, J. Y., et al., 2002. 1 : 250 000 Geological Report of Bangduo Area. Unpublished (in Chinese)
- Xu, R. K., Ci, Q., Pang, Z. J., et al., 2004. 1 : 250 000 Geological Report of Sinuowushan and Shiquanhe. Unpublished (in Chinese)
- Xu, Y. G., Menzies, M. A., Thirlwall, M. F., et al., 2001. Exotic Lithosphere Mantle beneath the Western Yangtze Craton: Petrogenetic Links to Tibet Using Highly Magnesian Ultrapotassic Rocks. *Geology*, 29(9): 863–866
- Yang, R. H., Li, C., Chi, X. G., et al., 2003. The Primary Study of Geochemical Characteristics and Tectonic Setting of Ophiolite in Yongzhu-Hamuhu, Tibet. *Geoscience*, 17(1): 14–19 (in Chinese with English Abstract)
- Ye, P. S., Wu, H. Z., Hu, D. G., et al., 2005. Geochemical Characteristics of Ophiolites in Yongzhu-Guomangcuo, Tibet and Its Tectonic Significance. *Geoscience*, 19(4): 508–514 (in Chinese with English Abstract)
- Ye, P. S., Wu, Z. H., Hu, D. G., et al., 2004. Geochemistry and Tectonic Setting of Ophiolite in West of Namco Lake, Tibet. *Geoscience*, 18(2): 237–248 (in Chinese with English Abstract)
- Yin, A., Harrison, T. M., 2000. Geologic Evolution of the Himalayan-Tibetan Orogen. *Annual Review of Earth and Planetary Sciences*, 28: 211–280
- Yu, H., 2011. Mineral Geochemical Characteristics and Genetic Mechanism of Olivine Rocks in Shangnan, Shanxi: [Dissertation]. China University of Geosciences (Beijing), Beijing (in Chinese with English Abstract)
- Zeng, Q. G., Mao, G. Z., Wang, B. D., et al., 2006. 1 : 250 000 Geological Report of Gaize with Geological Map. Unpublished (in Chinese)
- Zeng, Q. G., Mao, G. Z., Wang, B. D., et al., 2011. 1 : 250 000 Geological Report of Riganpeico. China University of Geoscience Press, Wuhan (in Chinese)
- Zhang, Y. X., 2007. Tectonic Evolution of the Middle-Western Bangong-Nujiang Suture, Tibet: [Dissertation]. Graduate School of the Chinese Academy of Sciences, Beijing (in Chinese with English Abstract)
- Zhang, Y. X., Zhang, K., Li, B., et al., 2007. Zircon SHRIMP U-Pb Geochronology and Petrogenesis of the Plagiogranites from the Lagkor Lake Ophiolite, Gerze, Tibet, China. *Chinese Science Bulletin*, 52: 651–659 (in Chinese)
- Zhao, J. H., Zhou, M. F., 2007. Geochemistry of Neoproterozoic Mafic Intrusions in the Panzhihua District (Sichuan Province, SW China): Implications for Subduction-Related Metasomatism in the Upper Mantle. *Precambrian Research*, 152: 27–47
- Zheng, L. L., Geng, Q. R., Dong, H., et al., 2003. The Discovery and Significance of the Relicts of Ophiolitic Mélanges along the Parlung Zangbo in the Bomi Region, Eastern Xizang. *Sedimentary Geology and Tethyan Geology*, 23: 27–30 (in Chinese with English Abstract)
- Zheng, Y. Y., Xu, R. K., He, L. X., et al., 2004. The Shiquan River Ophiolitic Mélange Zone in Xizang: the Delineation and Significance of a New Archipelagic Arc-Basin System. *Sedimentary Geology and Tethyan Geology*, 24: 13–20 (in Chinese with English Abstract)
- Zheng, Y. Y., Xu, R. K., Ma, G. T., et al., 2006. Ages of Generation and Subduction of Shiquan River Ophiolite: Restriction from SHRIMP Zircon Dating. *Acta Geologica Sinica*, 22(4): 895–904 (in Chinese with English Abstract)
- Zhu, D. C., Zhao, Z. D., Niu, Y., et al., 2011. The Lhasa Terrane: Record of a Microcontinent and Its Histories of Drift and Growth. *Earth and Planetary Science Letters*, 301: 241–255
- Zhu, D. C., Pan, G. T., Wang, L. Q., et al., 2008. Spatial-Temporal Distribution and Tectonic Setting of Jurassic Magmatism in the Gangdise Belt, Tibet, China. *Geological Bulletin of China*, 27(4): 458–468 (in Chinese with English Abstract)
- Zhu, Z., 2004. The Geochemical Characteristics and Tectonic Setting about Ophiolite in Yongzhu-Namucuo, Tibet Plateau: [Dissertation]. Jilin University, Changchun (in Chinese with English Abstract)